Hybrid Melittin Cytolytic Peptide-Driven Ultrasmall Lipid Nanoparticles Block Melanoma Growth *in Vivo*

Chuan Huang,[†,‡] Honglin Jin,[†,‡] Yuan Qian,[†,‡] Shuhong Qi,[†,‡] Haiming Luo,[†,‡] Qingming Luo,[†,‡] and Zhihong Zhang[†,‡,*]

[†]Britton Chance Center for Biomedical Photonics, Wuhan National Laboratory for Optoelectronics—Huazhong University of Science and Technology, Wuhan 430074, China, and [‡]MoE Key Laboratory for Biomedical Photonics, Department of Biomedical Engineering, Huazhong University of Science and Technology, Wuhan 430074, China

ABSTRACT The cytolytic peptide melittin is a potential anticancer candidate that may be able to overcome tumor drug resistance due to its lytic properties. However, *in vivo* applications of melittin are limited due to its main side effect, hemolysis, which is especially pronounced following intravenous administration. Here, we designed a hybrid cytolytic peptide, α-melittin, in which the N-terminus of melittin is linked to the C-terminus of an amphipathic α-helical peptide (α-peptide) *via* a GSG linker. The strong α-helical configuration allows α-melittin to interact with phospholipids and self-assemble into lipid nanoparticles, with a high efficiency for α-melittin encapsulation (>80%) and a strong ability to control the structure of the nanoparticle (~20 nm). This α-melittin-based lipid nanoparticle (α-melittin-NP) efficiently shields the positive charge of melittin (18.70 ± 0.90 mV) within the phospholipid monolayer, resulting in the generation of a neutral nanoparticle (2.45 ± 0.56 mV) with reduced cytotoxicity and a widened safe dosage range. Confocal imaging data confirmed that α-melittin peptides were efficiently released from the nanoparticles and were cytotoxic to the melanoma cells. Finally, α-melittin-NPs were administered to melanoma-bearing mice *via* intravenous injection. The growth of the melanoma cells was blocked by the α-melittin-NPs, with an 82.8% inhibition rate relative to the PBS-treated control group. No side effects of treatment were found in this study. Thus, the excellent properties of α-melittin-NP give it potential clinical applications in solid tumor therapeutics through intravenous administration.

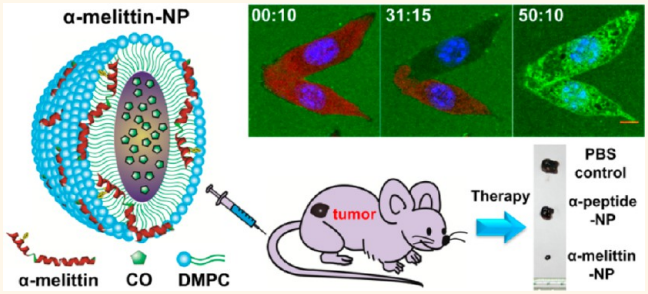

KEYWORDS: cytolytic peptide · melittin · nanoparticles · tumor therapy · cytotoxicity

Cytolytic peptides (*e.g.*, melittin, cecropins, and magainins) are considered to be one of the most potent anticancer drug candidates because their lytic properties may enable them to overcome tumor drug resistance.[1] Melittin, a 26 amino acid amphipathic cationic peptide (GIGAVLKVLTTGLPALISWIKRKRQQ-NH_2) derived from bee venom,[2] is able to interact with biological membranes due to its amphipathic properties.[3] Melittin can disrupt the phospholipid bilayer of cell membranes by forming transmembrane pores of widely distributed sizes that can be determined by temperature, pH, peptide concentration, ionic strength, and peptide-to-lipid ratios.[4] Melittin has shown some promise as a cancer therapeutic agent,[5−7] but *in vivo* applications of this peptide are limited due to its main side effect, hemolysis.[7−9]

In an effort to reduce hemolysis, the melittin sequence has been altered in some studies.[10−12] However, these alterations led to decreased membrane activity in cancer cells.[13] Other efforts have included conjugating melittin to an antibody or a targeting protein to increase the cancer cell specificity.[14,15] However, most melittin bioconjugates reported to date retain significant hemolytic activities, preventing them from being administered intravenously.

Many research groups have explored delivering melittin with nanoparticles. Polyethylene glycol-stabilized lipid disks,[16] poly(D,L-lactide-*co*-glycolide acid) nanoparticles,[17] and quantum dots[18] were all shown to be able to stably carry melittin. However, these nanoparticles are not suitable for systemic administration because surface loading of melittin does not shield its hemolytic nature, especially

* Address correspondence to czyzzh@mail.hust.edu.cn.

Received for review February 8, 2013 and accepted June 22, 2013.

Published online June 22, 2013
10.1021/nn400683s

during transport in the blood vessels.[16−18] Although liposomes have the ability to efficiently shield hydrophilic agents in their cores or hydrophobic agents in their phospholipid bilayer membranes,[19] they are not suitable for melittin delivery because their phospholipid bilayer membranes can be disrupted by melittin.[20] Recently, Soman *et al.* developed a melittin-carrying perfluorocarbon nanoemulsion with a phospholipid monolayer.[21] It showed for the first time melittin's ability to inhibit tumor growth after intravenous administration while mitigating the hemolytic activity of free melittin.[22] However, this melittin-loaded nanoparticle has a large size (~270 nm), rendering it inefficient to penetrate solid tumor,[23,24] has a variable surface charge (from −17.2 to 17.82 mV) associated with the melittin-loading content, and is unable to load additional chemotherapeutic agents into its solid core. Therefore, an ideal nanocarrier would have not only the ability to shield the cytotoxicity of melittin to safely deliver it systemically but also optimized physicochemical properties to enhance the utility rate and antitumor efficiency of the nanoparticle. These properties might include a small size so that the nanoparticle could penetrate the narrow collagen fibril space in solid tumors (20−40 nm),[25] a neutral charge so that the nanoparticle would not interfere with cationic or anionic proteins during systemic delivery, and synergistic loading of chemical agents for theranostic purposes.

Previously, we developed a 20 nm core−shell lipid nanoparticle, high-density lipoprotein (HDL)-mimicking peptide-phospholipid scaffold (HPPS) that has a structure and function that are precisely controlled by an amphipathic α-helical peptide (FAEKFKEAVKDYFAKFWD-NH_2).[26] This α-helical peptide constrains the phospholipid monolayer into its desired size by overcoming the high lipid curvature, whereas the embedded peptide retains the natural HDL receptor (scavenger receptor class B1, SR-B1) targeting function.[26] Therefore, given the α-helical nature of melittin and the need to shield its hemolytic side effects before it reaches the cancer site, we designed a novel hybrid cytolytic peptide in which the melittin peptide is linked with the C-terminus of another α-helical peptide (DWFKAFYDKVAEKFKEAF-NH_2,[27] denoted as α-peptide) through a GSG linker to generate DWFKAFYDKVAEKFKEAF-*GSG*-GIGAVLKVLTTGLPALISW-IKRKRQQ-NH_2, which is denoted as α-melittin. As shown in Scheme 1, α-melittin might tightly interact with phospholipids to deeply bury the cationic amino acid of melittin due to the nanostructural control ability of α-peptide. Especially, both the C-terminus of the α-peptide and the N-terminus of melittin contain hydrophobic amino acids, which are beneficial for deeply burying α-melittin within the phospholipid monolayer. Therefore, we presume that α-melittin not only is capable of precise structural control of lipid nanoparticles but also can shield the cytotoxicity of melittin through a highly self-assembled interaction with the phospholipid

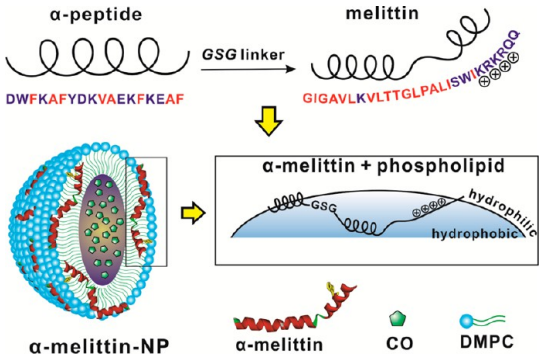

Scheme 1. Schematic diagrams of the α-melittin and α-melittin-NPs.

monolayer. We anticipate that α-melittin-based lipid nanoparticles (α-melittin-NPs) will inhibit tumor growth with few side effects *in vivo*.

RESULTS

To prepare α-melittin-NPs, a lipid emulsion was formed using 1,2-dimyristoyl-*sn*-glycero-3-phosphocholine (DMPC, 3 μmol) and cholesterol oleate (CO, 0.2 μmol). Then, an α-melittin solution (0.19 μmol, at a weight ratio of peptide to lipid of 0.5:1) was added into the lipid emulsion in a dropwise fashion and stored overnight at 4 °C until the turbid emulsion turned into a clear solution. The solution containing α-melittin-NPs was purified using a fast protein liquid chromatography (FPLC) system. The FPLC profile, in which both the 215 and 280 nm absorption curve represented the peptide/lipid-containing nanoparticle and the 215 nm absorption curve more sensitively reflected the peptide than the 280 nm absorption curve, showed that one narrow, main peak represented the desired α-melittin-NPs at a retention time of 62.4 min and that two impurity side peaks represented the large particles and the free peptide at retention times before 50 min and at 120 min, respectively (Figure 1A). The encapsulation rate of α-melittin in the nanoparticles, which was estimated by the ratio of the absorption value of the main peak area to the total peak area according to the FPLC profile at 215 nm, was very high (>80%). However, 0.19 μmol of α-peptide or melittin alone barely shrank the size of the lipid emulsion (data not shown). As a control, α-peptide-based lipid nanoparticles (α-peptide-NPs) were formed using 0.87 μmol of α-peptide (at a weight ratio of peptide to lipid of 1:1); the encapsulation rate of α-peptide in α-peptide-NPs was very low, and large amounts of free α-peptide were eluted out at a retention time of 122 min by FPLC (Supporting Information, Figure S1A). Even when the amount of melittin was increased to 0.87 μmol (at a weight ratio of peptide to lipid of 2.5:1), melittin alone remained unable to control the size of the lipid emulsion (Supporting Information, Figure S1B). When the mixture of 0.19 μmol of α-peptide and 0.19 μmol of

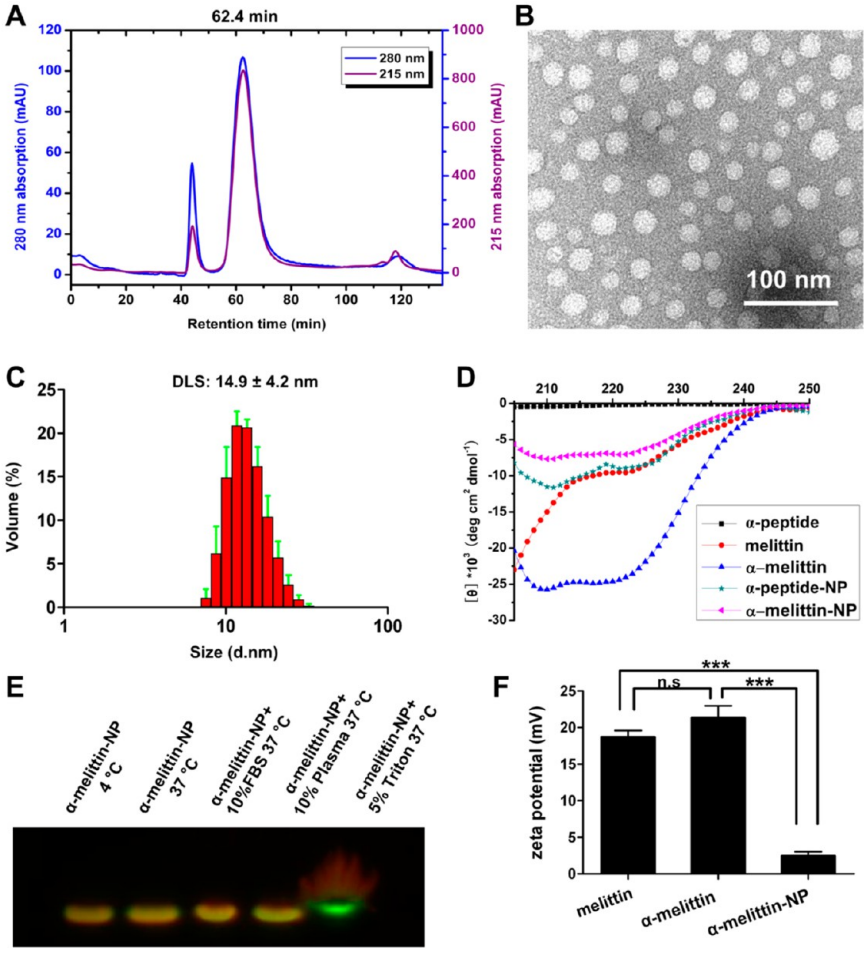

Figure 1. Characterization of α-melittin-NPs. (A) FPLC profile of α-melittin-NPs. (B) TEM image of α-melittin-NPs. (C) Size distribution of α-melittin-NPs as detected using DLS. (D) Circular dichroism spectra of α-peptide, melittin, α-melittin, α-peptide-NPs, and α-melittin-NPs in PBS solutions. (E) SDS-PAGE assay and fluorescence imaging evaluating the stability of the FITC-(DiR-BOA)α-melittin-NPs. (F) Zeta potential measurements of melittin, α-melittin, and α-melittin-NPs. Data are presented as the mean ± SD, $n = 3$, $^{***}p < 0.001$.

melittin was added to the lipid emulsion, the FPLC profile showed a poor encapsulation rate for the peptides and a low productivity rate for the nanoparticles (Supporting Information, Figure S1C).

Next, we measured the physicochemical properties of α-melittin-NPs. The transmission electron microscopy (TEM) data clearly showed that α-melittin-NPs are sub-30 nm spherical nanoparticles with perfect monodispersity (Figure 1B). Dynamic light scattering (DLS) data indicated that the size of the nanoparticles was 14.9 ± 4.2 nm ($n = 3$), with a narrow size distribution (Figure 1C). Thus, melittin connected to α-peptide not only retained the ability to control the size of the nanoparticles but also drastically increased the utility rate of peptides and enhanced the self-assembled interaction of the peptide and phospholipid.

The secondary structures of α-melittin and α-melittin-NPs were analyzed by measuring the circular dichroism (CD) spectrum. The data revealed that both α-melittin-NPs and α-peptide-NPs display the characteristics of α-helical configurations, with double negative peaks at 222 and 208 nm (Figure 1D). Interestingly, the secondary structure of α-melittin was distinctive from that of α-peptide and melittin in PBS solution; α-melittin displayed a strong α-helical configuration even in the absence of lipid. To confirm the core-loading ability of α-melittin-NPs, Fluo-BOA was used as a model cargo and was loaded into the core of α-melittin-NPs. The FPLC profile of (Fluo-BOA)α-melittin-NPs showed that the 488 nm absorption peak of Fluo-BOA exactly matched the α-melittin-NP peak at 280 nm (Supporting Information, Figure S2A). To verify the stability of α-melittin-NPs, we prepared dual-labeled α-melittin-NP, in which α-melittin was labeled with fluorescein isothiocyanate (FITC) and the core was loaded with DiR-BOA (1,1′-dioctadecyl-3,3,3′,3′-tetramethylindotricarbocyanine iodide bisoleate, a lipid-anchored near-infrared fluorophore), denoted as FITC-(DiR-BOA)α-melittin-NP. The FPLC profile of FITC-(DiR-BOA)α-melittin-NPs confirmed that both FITC and DiR-BOA were successfully loaded on the nanoparticles, which was evidenced by the absorption peaks of 495 nm for

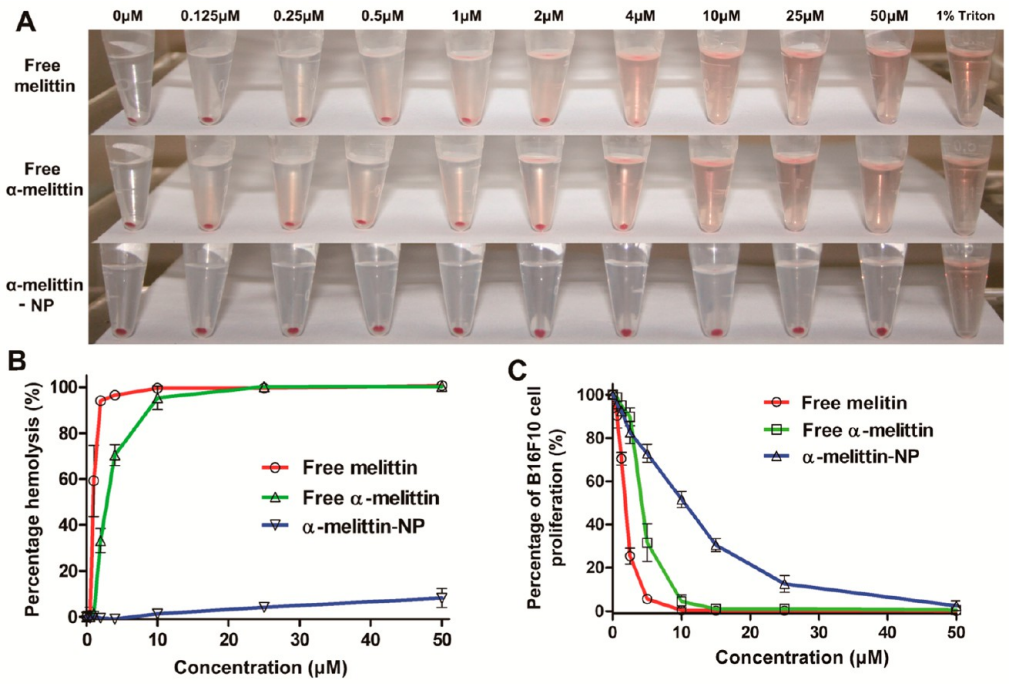

Figure 2. α-Melittin-NP cytotoxicity assays in RBC and cultured melanoma cells *in vitro*. (A, B) Hemolysis assays for melittin, α-melittin, and α-melittin-NPs in RBC. (C) Proliferation assays evaluating the cytotoxicity of melittin, α-melittin, and α-melittin-NPs in tumor cells. Data are presented as the means ± SD, *n* = 3.

FITC and 700 nm for DiR-BOA matching with the 280 nm absorption peaks of α-melittin-NPs (Supporting Information, Figure S2B). The semi-native SDS-PAGE data indicated that FITC-(DiR-BOA)α-melittin-NPs were stable in 10% FBS or 10% plasma at 37 °C for 3 h, as both FITC and DiR-BOA fluorescent signals were detected on the same band. As a control, adding 5% Triton induced nanoparticle decomposition, resulting in the leakage of DiR-BOA from the nanoparticles and the separation of FITC and DiR-BOA fluorescent signals. Furthermore, the peptide release assay and the long-term storage stability test indicated that α-melittin tightly interacted with phospholipid to maintain the size stability of the nanoparticles (Supporting Information, Figures S4 and S5).

The most important property of the α-melittin-NPs is that the large positive charges of melittin (18.70 ± 0.90 mV, *n* = 3) and α-melittin (21.33 ± 1.64 mV, *n* = 3) are shielded and result in the nanoparticles having an approximately neutral zeta potential (2.45 ± 0.56 mV, *n* = 3) (Figure 1F). This result strongly suggests that the cationic α-melittin peptide was deeply buried in the phospholipid monolayer of the nanoparticle and that this burial is critical to reduce the cytotoxicity of melittin.

To test this hypothesis, hemolysis assays were performed *in vitro* using red blood cells (RBC). As shown in Figure 2A and B, very low concentrations of melittin (4 μM) or α-melittin (10 μM) induced complete lysis of RBC, whereas 50 μM (peptide concentration) α-melittin-NPs induced minimal hemoglobin release (8 ± 4%, *n* = 3). Next, malignant melanoma B16F10 cells were used as a model to assess the cytotoxicity of α-melittin-NPs in tumor cells. Compared with the half-maximal inhibitory concentrations (IC_{50}) of free melittin (1.71 ± 0.04 μM) and α-melittin (4.20 ± 0.09 μM), α-melittin-NPs appeared to decrease tumor cells' cytotoxicity, as indicated by an increased IC_{50} value of 11.26 ± 1.37 μM (Figure 2C). To further confirm the differential cytotoxicity of α-melittin-NPs to RBC and B16F10 cells, the cells were incubated with FITC-(DiR-BOA)α-melittin-NPs for 1 h at 37 °C and the fluorescent signals in cells were detected using flow cytometry. The strong fluorescent signals of both FITC and DiR-BOA were observed in B16F10 cells, whereas these signals were seldom detected in RBC (Supporting Information, Figure S6). Thus, α-melittin buried within the lipid layer of nanoparticles results in reduced toxicity to RBC and reduced efficiency in killing tumor cells *in vitro* at concentrations ranging from 10 to 50 μM. These properties are beneficial for the *in vivo* utility of α-melittin-NPs and indicate that these nanoparticles have a favorable safety profile.

To assess the release of α-melittin from the nanoparticles, B16F10 cells were incubated with FITC-(DiR-BOA)α-melittin-NPs for 2 h at 37 °C and then stained with Hoechst 33342. Confocal imaging data showed that both FITC and DiR-BOA signals were detected in B16F10 cells. The fluorescent signals of FITC and DiR-BOA were separated, and some cells appeared dead by morphology and nucleus changes (Figure 3A). These data indicated that FITC-(DiR-BOA)α-melittin-NPs entered

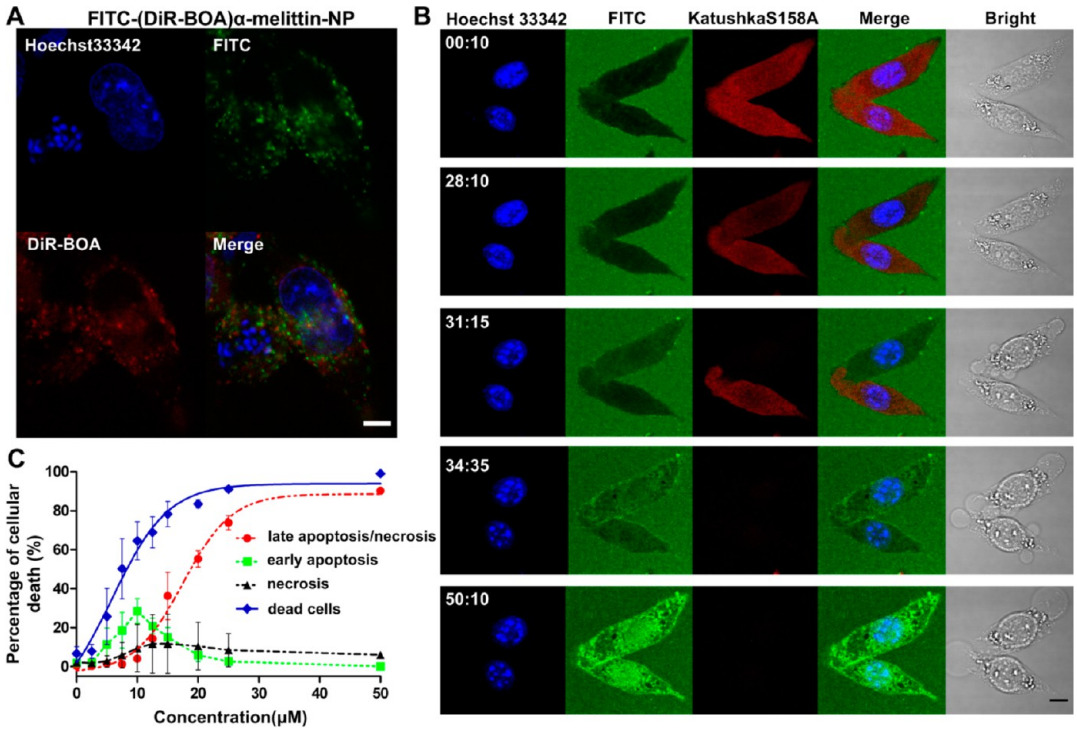

Figure 3. Imaging and quantitative analyses of α-melittin-NP cytotoxicity in melanoma cells. (A) Confocal imaging of B16F10 melanoma cells incubated with FITC-(DiR-BOA)α-melittin-NPs for 2 h and stained with Hoechst 33342. Bar = 5 μm. (B) Real-time visualization of the α-melittin-NPs attacking the tumor cells that were obtained using confocal microscopy. Scale bar = 10 μm. (C) Flow cytometric quantitative analyses of the mortality rates of B16F10 cells that had been treated with α-melittin-NPs at different concentrations. Data are presented as the mean ± SD, *n* = 3.

into the B16F10 cells, and the anticancer agent α-melittin peptides were released from the nanoparticles and functionalized. To visually demonstrate the effects of α-melittin-NPs on tumor cells, B16F10 cells expressing KatushkaS158A[28] (B16-KatushkaS158A), a tetrameric far-red fluorescent protein, were stained with the nuclear dye Hoechst33342 and were treated with fluorescein-labeled α-melittin-NPs (FITC-α-melittin-NPs) (Supporting Information, Figure S2C). Using confocal microscopy, changes in cell morphology and three-color fluorescence signals were imaged at 5 s intervals (Figure 3B and Supporting Information, Video S1). At the beginning of the treatment of B16-KatushkaS158A with 25 μM (peptide concentration) FITC-α-melittin-NPs, the B16-KatushkaS158A cells showed a strong far-red fluorescent signal in the cytosol. The FITC signal was excluded from the cells and some recruitment on the cell membrane. After 28 min of treatment with FITC-α-melittin-NPs, the far-red signal in the cells gradually decreased, suggesting that the FITC-α-melittin released from the nanoparticles generated the pores on the cell membrane and allowed KatushkaS158A (~120 kDa) to leak out of the cells. As time progressed, the KatushkaS158A fluorescence signal completely disappeared from the cells. Meanwhile, the FITC signal increased in the intracellular region, with the FITC signal being especially strong on the endomembrane system. The chromosomes were observed to have condensed and ruptured, and the cell morphology became altered as more and larger bubbles formed (Figure 3B).

Next, we investigated the concentration-dependent cytotoxicity of α-melittin-NPs and the mechanism underlying cell death. B16F10 cells were treated with various concentrations of α-melittin-NPs for 3 h and then stained with annexin V-FITC/PI for flow cytometry analysis. As shown in Figure 3C and in Figure S7A of the Supporting Information, low concentrations (5−10 μM) of α-melittin-NPs primarily induced early apoptosis in B16F10 cells (lower-right quadrant of the scatter plot), and high concentrations (>12.5 μM) of α-melittin-NPs primarily resulted in B16F10 cell necrosis (upper-right quadrant of the scatter plot). When the concentration of α-melittin-NPs was below 2.5 μM, the α-melittin-NPs did not damage B16F10 cells, even after incubation for 24 h (Supporting Information, Figure S7B). These results further suggested that intravenous injection may allow α-melittin-NPs to retain their cytotoxicity to tumor cells following the selective accumulation of α-melittin-NPs in the tumor region due to the enhanced permeability and retention (EPR) effect. In addition, intravenous injection of α-melittin-NPs might prevent side effects as a result of low concentration of α-melittin-NPs in normal tissues.

To evaluate the efficacy of α-melittin-NPs against B16F10 melanoma *in vivo*, 20 mg/kg (3.7 μmol/kg of peptide) of α-melittin-NPs were injected into tumor-bearing mice *via* the tail vein on the fifth, seventh,

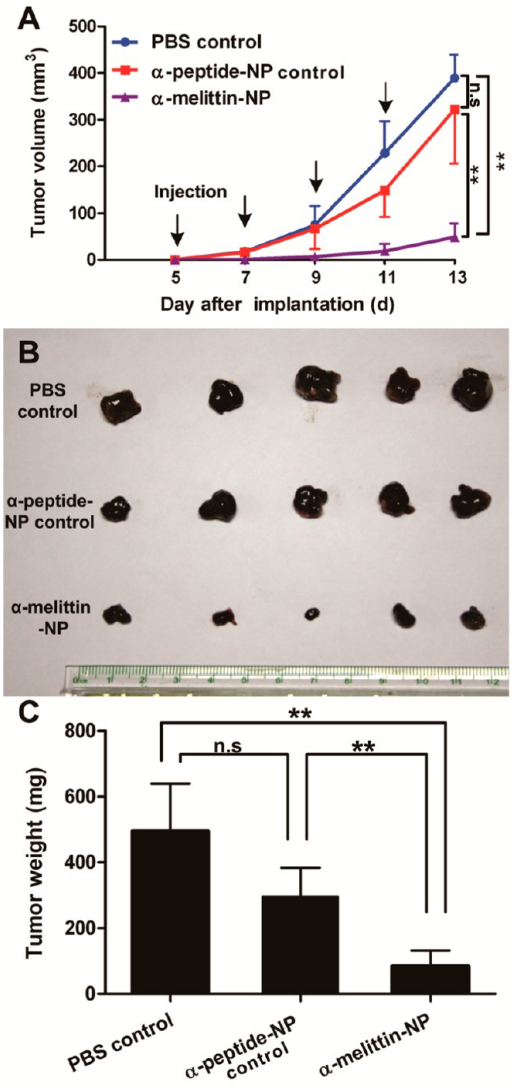

Figure 4. ***In vivo*** **evaluation of the effect of α-melittin-NPs on the inhibition of melanoma growth. (A) Tumor volume in each group with increasing days. Tumor volume in the α-melittin-NP-treated group was significantly inhibited compared to the other groups. (B) Photographs and (C) weights of the tumors from each group on the 13th day. Data are presented as the means ± SD,** $n = 5$, $^{**}p < 0.01$.

ninth, and 11th days after 8×10^5 B16F10 cells had been subcutaneously implanted into C57/BL6 mice. Tumor-bearing mice that had been injected intravenously with α-peptide-NPs and PBS served as the control groups. As shown in Figure 4A and in Figure S8 of the Supporting Information, the mean tumor volumes differed significantly between the α-melittin-NP-treated group (48.89 ± 29.50 mm^3) and the α-peptide-NP-treated group (322.20 ± 116.67 mm^3) or the PBS-treated group (389.23 ± 49.84 mm^3) on the 13th day after the implantation of tumor cells ($p < 0.01$, $n = 5$). Both the images and weights of the tumor xenografts further confirmed the efficient inhibition of tumor growth by the α-melittin-NPs (85.04 ± 47.01 mg), with an 82.8% inhibition rate relative to the PBS-treated control group (495.28 ± 144.56 mg) and a 71.4% inhibition rate relative to the α-peptide-NP control group (297.30 ± 86.60 mg) (Figure 4B and C, $n = 5$, $p < 0.01$).

To evaluate the side effects of α-melittin-NPs, blood was collected from the mice on the 13th day of tumor growth for hemanalysis and biochemical analyses, and normal tissues (hearts, livers, spleens, lungs, and kidneys) were removed for histopathologic analyses. There were no differences in the number of white and red blood cells (WBC and RBC), hemoglobin (HGB), mean cell hemoglobin (MCH), mean corpuscular hemoglobin concentrations (MCHC), and hepatic and renal function parameters (*e.g.*, blood urea nitrogen (BUN), total bilirubin (T-Bil), and glutamate pyruvate transaminase (ALT)) among the three groups (Figure 5, Table S1 in the Supporting Information). The only difference observed was that the aspartate aminotransferase (AST) levels in the α-melittin-NP-treated group (197.20 ± 34.47 U/L) were lower than those in both the PBS-treated control (543.60 ± 137.14 U/L) ($p < 0.01$, $n = 5$) and α-peptide-NP-treated control (402.40 ± 189.39 U/L) ($p < 0.05$, $n = 5$). AST, an important liver enzyme, was elevated in the PBS-treated control and α-peptide-NP-treated control groups (normal values of AST are 111.25 ± 19.92 U/L in female mice), perhaps as a result of liver injury that had been induced by tumor growth. This damage was confirmed by conducting histopathologic analyses of the tissues (Figure 6). Images of H&E-stained tissue sections showed that many vacuoles appeared in the hepatic cells in the PBS-treated control group but did not appear in the α-melittin-NP- or the α-peptide-NP-treated groups. No histopathological abnormities or lesions were found in the other organs (hearts, spleens, lungs, and kidneys) in the three groups. These results indicated that α-melittin-NPs inhibited tumor growth and simultaneously reduced liver injury. In addition, it is worth mentioning that there were no differences in serum hemoglobin or the weights of the mice among the three groups (Figure 5C and J), indicating that α-melittin-NPs can be used safely *in vivo* without toxicity.

DISCUSSION

The central purpose of the present study was to develop a simple and biocompatible melittin-carrying nanoparticle that could overcome the toxicity of melittin in the vascular system and normal tissues while retaining melittin-induced toxicity in tumors. We designed a novel hybrid melittin cytolytic peptide that had a strong α-helical configuration and could be used to form an ultrasmall lipid nanoparticle that had the ability to inhibit tumor growth. Our results strongly support our designs for the α-melittin cytolytic peptide and the α-melittin-based lipid nanoparticle.

The α-melittin cytolytic peptide was hybridized using a unique fusion approach in which the N-terminus of melittin was linked to the C-terminus of α-peptide

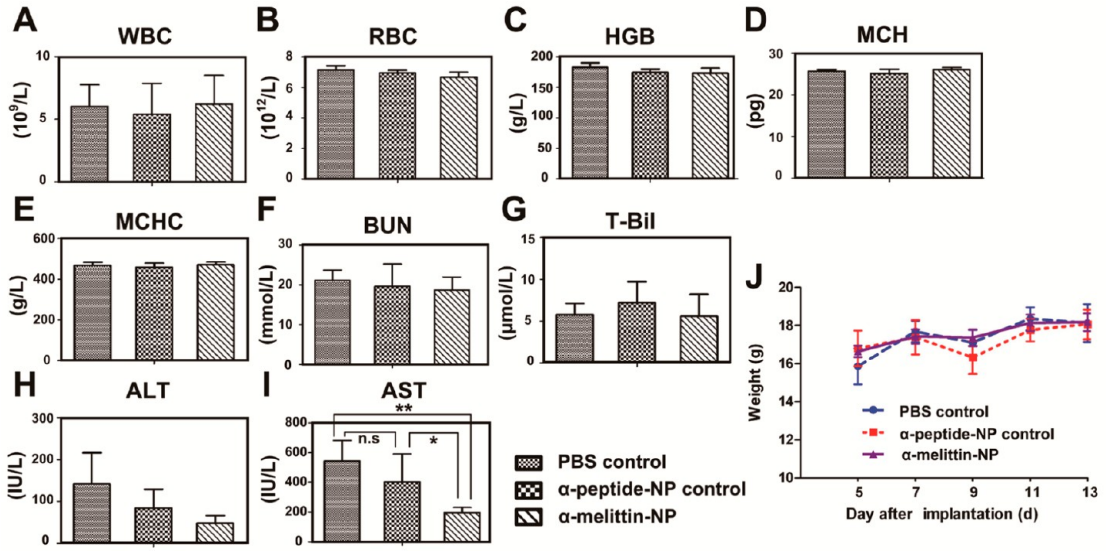

Figure 5. Evaluation of the side effects of α-melittin-NPs *in vivo*. (A−E) Blood hemanalysis of white blood cells (WBC), red blood cells (RBC), hemoglobin (HGB), mean cell hemoglobin (MCH), and mean corpuscular hemoglobin concentration (MCHC). (F−I) Biochemical analyses of blood urea nitrogen (BUN), total bilirubin (T-Bil), glutamate pyruvate transaminase (ALT), and glutamic-oxalacetic transaminase (AST). (J) Line plot of body weight changes in tumor-bearing mice during treatment. Data are presented as the means ± SD, $n = 5$, $^{*}p < 0.05$, $^{**}p < 0.01$.

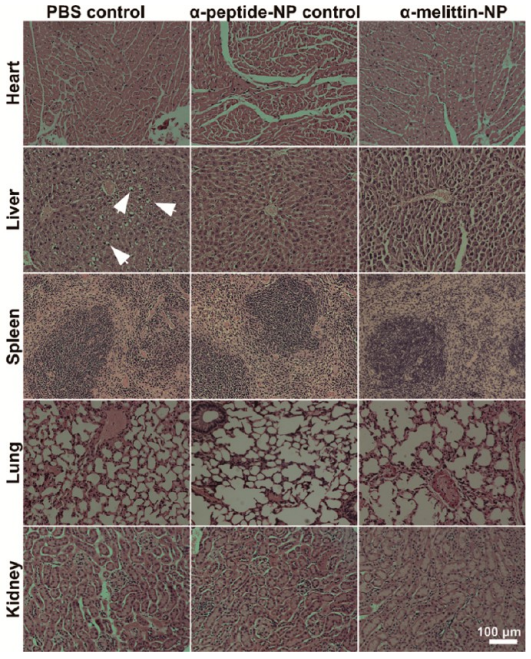

Figure 6. Histopathologic analyses of H&E-stained tissue sections from the hearts, livers, spleens, lungs, and kidneys of tumor-bearing mice. Arrows indicate damaged liver cells.

through a *GSG* linker. Because the cytotoxicity functional domain of melittin is located at the C-terminus,[13] this fusion should allow melittin to remain free to function. The N-terminus of melittin contains several hydrophobic amino acids (GIGAVL). Thus, we chose α-peptide (DWFKAFYDKVAEKFKEAF-NH_2), which contains two hydrophobic amino acids (AF) at the C-terminus, to link to the N-terminus of melittin, thereby increasing the probability of deeply burying melittin in the lipid layer of the nanoparticle (Scheme 1). We hoped that α-melittin could be efficiently encapsulated within the lipid nanoparticle with the aid of the structural control ability of α-peptide and that α-melittin could be released from the nanoparticles to exert cytotoxicity to the tumor cells.

Surprisingly, α-melittin appeared to display enhanced synergistic functions in the formation of the lipid nanoparticle, with a higher encapsulation rate and stronger nanostructural control compared with α-peptide. There were several lines of evidence that supported this idea: (1) a high encapsulation rate (>80% of α-melittin was encapsulated into the nanoparticle) and (2) lower peptide dosage and smaller nanosize (α-melittin controlled the size of the nanoparticles more efficiently than did α-peptide). The required molar ratios were 0.19/3 for α-melittin/lipid and 0.87/3 for α-peptide/lipid, respectively. The size of the α-melittin-NPs was also smaller than that of the α-peptide-NPs when the same molar ratio of peptide to DMPC/CO was used. Also supporting this is (3) enhanced α-helical conformation: Interestingly, melittin and α-peptide alone do not form typical α-helical conformations in PBS solution. When melittin is linked with α-peptide, it displays a strong α-helical conformation. Both α-melittin-NPs and α-peptide-NPs displayed a typical α-helical structure. Moreover, α-melittin-NPs have many advantages, such as neutral charge, ultrasmall size, stability, and a core−shell structure that allows core loading of oleate-modified imaging agents (*e.g.*, Fluo-BOA and DiR-BOA).

Compared to free melittin, α-melittin-NPs clearly increased the concentration of α-melittin required for cytotoxicity, resulting in a widening of the safe dosage

range of α-melittin. In the present study, the therapeutic dosage of α-melittin-NPs *in vivo* was 20 mg/kg. We found that there was no obvious toxicity when α-melittin-NPs were administered intravenously at dosages below 70 mg/kg, whereas the median lethal dose (LD_{50}) of free melittin was 3−4 mg/kg.[29]

We found that α-melittin-NP-mediated inhibition of tumor growth occurs in a concentration-dependent manner rather than *via* SR-B1-mediated targeting. Although α-melittin-containing α-peptide has the potential for SR-B1 targeting, we did not find evidence of SR-B1 targeting in this study. α-melittin-NPs also obviously inhibit the proliferation of human nasopharyngeal carcinoma 5−8F cells[30] ($SR\text{-}B1^+$) and human fibrosarcoma HT1080 cells[26] ($SR\text{-}B1^-$), in which the cytotoxicity was not well correlated with the cellular SR-B1 expressing level (data not shown). It is interesting to observe that the cytotoxicities of α-melittin-NPs to tumor cells and RBC were significantly different, as 50 μM α-melittin-NPs induced only 8% RBC to hemolyze, while causing 98% of B16F10 tumor cells to die (Figure 2B and C). Through comparison of the binding or entering ability of FITC-(DiR-BOA)α-melittin-NPs between B16F10 cells and RBC using flow cytometry, we confirmed that the cytotoxicity of α-melittin-NPs was correlated with the binding or entering efficiency of α-melittin to the cells (Supporting Information, Figure S6). However, why are α-melittin-NPs easier to bind and why do they enter into tumor cells more easily than RBC? The potential reason might be due to the different amount of cholesterol on the cell membrane of tumor cells and RBC.[31] The cell membrane of RBC containing abundant cholesterol may limit the phospholipid exchange between the monolayer phospholipids of nanoparticles and bilayer phospholipids of cell membranes or prevent α-melittin peptide transference from nanoparticle to cells. The precise mechanism of α-melittin-NPs in exerting different cytotoxicity between tumor cells and RBC is unclear.

On the basis of all of these characteristics of α-melittin-NPs, we speculate that there are two potential advantages to the use of α-melittin-NPs in tumor therapeutics *in vivo*. First, the ultrasmall size of α-melittin-NPs is beneficial for diffusion and penetration of the nanoparticle in solid tumors, which exist as compact collagen fibrils with narrow spaces (20−40 nm).[23,25] Second, the core−shell structure of the nanoparticles can be core-loaded with imaging agents[26,32,33] and therapeutic agents (*e.g.*, paclitaxel oleate),[34] increasing the ease of achieving synergistic therapeutics for tumors.[35]

CONCLUSIONS

In summary, we designed a novel hybrid melittin cytolytic peptide and created a novel approach to encapsulating melittin in a biocompatible lipid nanoparticle. Our data demonstrated that the positive charge of α-melittin and its cytotoxicity are successfully shielded within ultrasmall lipid nanoparticles. α-Melittin can also be released to exert its cytotoxic effects on tumor cells. α-Melittin-NPs administered *via* intravenous injection efficiently inhibited tumor growth with few side effects. Furthermore, several attractive characteristics of α-melittin-NPs, such as their ultrasmall size (~20 nm), which allows them to efficiently penetrate solid tumors, their stable neutral charge, which allows them to avoid interference from cationic or anionic proteins, their core−shell spherical morphology, which enables the synergistic loading of chemical agents, and their perfect biocompatibility and monodispersity, give α-melittin-NPs superior utility as synergistic therapeutics for solid tumors.

MATERIALS AND METHODS

General Comments. 1,2-Dimyristoyl-*sn*-glycero-3-phosphocholine was purchased from Avanti Polar Lipids Inc. (Alabaster, AL, USA). Cholesteryloleate, fluorescein isothiocyanate, and Hoechst33342 were obtained from Sigma-Aldrich Co. (St. Louis, MO, USA). Fluo-BOA, which consists of two oleoyl groups conjugated to a hydrophilic fluorescein dye, was generated as previously described.[26,36] The melittin, α-peptide, and α-melittin peptides were synthesized by Apeptide Co., Ltd. (Shanghai, China).

Preparation of Nanoparticles and Concentration Measurements. The α-melittin-NPs and α-peptide-NPs were prepared as follows. (1) A mixture of DMPC and CO in chloroform was dried under nitrogen to form a uniform lipid film. (2) Phosphate-buffered saline (PBS) solution was added, and the mixture was vortexed and sonicated for 1 h at 48 °C to form a lipid emulsion. (3) The peptides were added to the lipid emulsion in a dropwise fashion and then stored overnight at 4 °C. To prepare the nanoparticles that were core-loaded with Fluo-BOA or DiR-BOA, the only difference in the protocol was the first step, in which Fluo-BOA or DiR-BOA was mixed with DMPC and CO in chloroform. To prepare the FITC-α-melittin-NPs or FITC-(DiR-BOA)-α-melittin-NPs, fluorescein isothiocyanate was conjugated to the lysine residues of the peptides after the α-melittin-NPs or (DiR-BOA)α-melittin-NPs had been prepared. All of the nanoparticles were purified using a fast protein liquid chromatography system with a HiLoad 16/60 Superdex 200 pg column (General Electric Healthcare, NY, USA) and then concentrated to the desired concentrations. In the present study, the concentrations were calculated from the peptide concentrations, which were measured in the aqueous phase of the solution extracted from the nanoparticles using a CBQCA protein quantitation kit (cat. no. MP 0667, Invitrogen Corporation, CA, USA).

Measurement of the Physicochemical Properties of the Nanoparticles. Transmission electron microscopy was performed using a TECNAI G_2 (FEI Company, OR, USA) to determine the morphology of the α-melittin-NPs, which were negatively stained with 1% uranyl acetate prior to imaging. The particle size distributions and zeta potentials of the α-melittin-NPs were measured using dynamic light scattering photon correlation spectroscopy on a Zetasizer Nano-ZS90 (Malvern Instruments, Worcestershire, UK).

Measurement of the Circular Dichroism Spectra. The CD spectra of the peptide and nanoparticles were measured from 190 to 250 nm with a Jasco J-810 circular dichroism spectropolarimeter (Tokyo, Japan).

Stability Evaluation. FITC-(DiR-BOA)α-melittin-NPs were incubated with PBS, 10% FBS, 10% plasma, and 5% Triton for 3 h at 37 °C.

The stability of the α-melittin-NPs was analyzed and evaluated using SDS-polyacrylamide gel electrophoresis (SDS-PAGE) with an 8% semi-native gel and a custom-made optical fluorescence imaging system that had been fitted with a green filter set (excitation filter: 469/35 nm; emission filter: 510/42 nm), a near-infrared filter set (excitation filter: 716/40 nm; emission filter: 800/40 nm), and a 150 W xenon lamp (Crownteck, Inc., PA, USA).[37,38]

Hemolysis Assays. Fresh mouse blood was collected in anticoagulant tubes with EDTA·2K. The red blood cells were separated, purified, and diluted to 5.0×10^7/mL for the hemolysis assays. Various concentrations of free melittin, free α-melittin, and α-melittin-NPs were incubated with 100 μL of RBC at 37 °C for 3 h. The absorbance of the supernatants from each group of RBC was measured using a microplate reader (model 525, TECAN Group Ltd., Männedorf, Switzerland) at 540 nm. RBC that had been treated with 1% Triton were used as a positive control, and the release rate of hemoglobin for this group was set at 100%.

Cell Culture. B16F10 melanoma cells were purchased from Boshide Biology Ltd. (Wuhan, China). The cells were cultured in RPMI-1640 medium (HyClone, Thermo Fisher Scientific, Beijing, China) containing 100 U/mL of penicillin−streptomycin (Gibco, Life Technologies, Carlsbad, CA, USA) and 10% fetal bovine serum (FBS, HyClone). The cells were grown at 37 °C in an incubator with a 5% CO_2, humidified atmosphere.

Cell Proliferation Assays. B16F10 cells (3.0×10^3 per well) were seeded in 96-well plates and were incubated for 48 h. Various concentrations of melittin, α-melittin, and α-melittin-NPs were added to the wells and were incubated with B16F10 cells for 3 h at 37 °C. The cells were washed with PBS to remove the drugs, after which point they continued to be cultured for 45 h at 37 °C. The cell proliferation assays were performed using the Cell Counting Kit 8 (CCK-8, Dojindo Molecular Technologies, Inc., Kumamoto, Japan).

Confocal Imaging. To illustrate the peptide release and delivery mode of the α-melittin-NPs, B16F10 cells or B16-KatushkaS158A cells (3×10^4 per well) were seeded into the 35 mm culture dishes with a cover glass bottom (NEST Biotechnology Co. Ltd., Shanghai, China) and were incubated for 48 h at 37 °C. Subsequently, FITC-(DiR-BOA)α-melittin-NPs were added to the dishes containing B16F10 cells and FITC-α-melittin-NPs (25 μM) were added to the dishes containing the B16-KatushkaS158A cells. Prior to confocal imaging, the cells were stained with Hoechst33342 for 10 min and were washed twice. The fluorescence signals were detected using an Olympus FV1000 confocal laser scanning microscope (Olympus, Tokyo, Japan) at excitation wavelengths of 405 nm for Hoechst33342, 488 nm for Fluo-BOA and FITC, 543 nm for KatushkaS158A, and 633 nm for DiR-BOA.

Cell Death Flow Cytometry Assays. An annexin-V-FITC/PI kit (Sungene Biotech Co., Ltd., Tianjin, China) was used to determine the mechanism underlying α-melittin-NP-induced cell death. B16F10 cells (2×10^4 per well) were seeded in a 24-well plate and were incubated for 48 h at 37 °C. The cells were harvested after incubation with α-melittin-NPs at 0, 2.5, 5, 7.5, 10, 12.5, 15, 20, 25, or 50 μM for 3 h at 37 °C and were then stained with annexin-V-FITC and PI solution for 5 min. The dual fluorescent signals of the cells were analyzed using a microcapillary flow cytometer (Guava EasyCyte8HT, EMD Millipore Corporation, Billerica, MA, USA).

***In Vivo* Antitumor Studies.** All animal studies were performed in compliance with protocols that had been approved by the Hubei Provincial Animal Care and Use Committee and the experimental guidelines of the Animal Experimentation Ethics Committee of Huazhong University of Science and Technology. C57BL/6 mice (female, 6 weeks old) were implanted subcutaneously with 8×10^5 B16F10 melanoma cells in the left flank. The day of tumor cell implantation was defined as day 0. On the fifth day after implantation of the tumor cells, the mice were randomly separated into 3 groups. Each group contained 5 mice. The tumor-bearing mice were administrered α-melittin-NPs (20 mg/kg), α-peptide-NPs (at the same molarity as the α-melittin NPs), or PBS *via* tail vein injection, every other day for a total of 4 doses. The body weight and tumor size of each mouse were measured using an electronic balance and calipers on the fifth, seventh, ninth, 11th, and 13th days. The tumor volumes were calculated according to the following formula: $V = 0.5 \times L(\text{length}) \times W(\text{width}) \times H(\text{height})$. On the 13th day, all of the mice were killed, and the tumors were dissected, photographed, and weighed. The inhibition rates of tumor growth were calculated according to the following formula: inhibition (%) = $(C - T)/C$, where C was the average volume of the tumor in the control group (PBS- or α-peptide-NP-treated) and T was the average volume of the tumor in the α-melittin-NP-treated group.

Histopathologic Analyses of Normal Tissues. The hearts, livers, spleens, lungs, and kidneys were extracted from tumor-bearing mice and fixed in a 4% paraformaldehyde solution. The organs were embedded in paraffin, sectioned, and stained with hematoxylin and eosin (H&E). The images were obtained using a BX53 microscopy system (Olympus, Tokyo, Japan) that was equipped with a color CCD (DMK 41BU02, Sony Co., Tokyo, Japan)

Blood Hemanalysis and Biochemical Analyses. Blood samples were collected before the mice were killed. The blood cell and biochemical analyses were performed using a hematology analyzer (BC-3200, Mindray, Shenzhen, China) and a biochemical analyzer (SPOTCHEM EZ SP-4430, Arkray Inc., Kyoto, Japan), respectively.

Statistics. Nonparametric statistics (Kruskal−Wallis and Mann−Whitney U tests) were used to determine significant differences for the *in vivo* studies, and Student's *t* test (two tailed) was used for the *in vitro* studies. Significant differences between or among groups were indicated by * for $p < 0.05$, ** for $p < 0.01$, and *** for $p < 0.001$.

Conflict of Interest: The authors declare no competing financial interest.

Supporting Information Available: FPLC profiles of nanoparticles based on different peptides. FPLC profiles of fluorescently labeled α-melittin-NPs. Scatter plots of flow cytometry assays examining the cytotoxicity of α-melittin-NPs in melanoma cells. Photos of tumor-bearing mice after 13 days of treatment with α-melittin-NPs and α-peptide-NPs or PBS control. Semi-native SDS-PAGE assay and fluorescence imaging to evaluate the stability of FITC-(DiR-BOA)α-melittin-NP. Safety evaluation of α-melittin-NPs for *in vivo* applications. This material is available free of charge *via* the Internet at http://pubs.acs.org.

Acknowledgment. We thank Dr. Gang Zheng (University of Toronto, Toronto, ON, Canada) for paper discussion and providing Fluo-BOA and DiR-BOA. We thank the Analytical and Testing Center (Huazhong University of Science and Technology, HUST) for spectral measurements. We thank the facility support of the Center for Nanoscale Characterization & Devices (CNCD, Tecnai G20 U-Twin), WNLO-HUST. This work was supported by the National Basic Research Program of China (Grant No. 2011CB910401), Science Fund for Creative Research Group of China (Grant No. 61121004), National Natural Science Foundation of China (Grant No. 81172153), and National Science and Technology Support Program of China (Grant No. 2012BAI23B02).

REFERENCES AND NOTES

1. Papo, N.; Shai, Y. Host Defense Peptides as New Weapons in Cancer Treatment. *Cell. Mol. Life Sci.* **2005**, *62*, 784–790.
2. Habermann, E. Bee and Wasp Venoms. *Science* **1972**, *177*, 314–322.
3. Dempsey, C. E. The Actions of Melittin on Membranes. *Biochim. Biophys. Acta, Rev. Biomembr.* **1990**, *1031*, 143–161.
4. Raghuraman, H.; Chattopadhyay, A. Melittin: A Membrane-Active Peptide with Diverse Functions. *Biosci. Rep.* **2007**, *27*, 189–223.
5. Oršolić, N. Potentiation of Bleomycin Lethality in HeLa and V79 Cells by Bee Venom. *Arch. Ind. Hyg. Toxicol.* **2009**, *60*, 317–326.
6. Oršolić, N. Bee Venom in Cancer Therapy. *Cancer Metastasis Rev.* **2012**, *31*, 173–194.
7. Liu, S.; Yu, M.; He, Y.; Xiao, L.; Wang, F.; Song, C.; Sun, S.; Ling, C.; Xu, Z. Melittin Prevents Liver Cancer Cell Metastasis through Inhibition of the Rac1-Dependent Pathway. *Hepatology (Hoboken, NJ, U. S.)* **2008**, *47*, 1964–1973.

8. Hoshino, Y.; Kodama, T.; Okahata, Y.; Shea, K. J. Peptide Imprinted Polymer Nanoparticles: A Plastic Antibody. *J. Am. Chem. Soc.* **2008**, *130*, 15242–15243.
9. Hoshino, Y.; Urakami, T.; Kodama, T.; Koide, H.; Oku, N.; Okahata, Y.; Shea, K. J. Design of Synthetic Polymer Nanoparticles that Capture and Neutralize a Toxic Peptide. *Small* **2009**, *5*, 1562–1568.
10. Zhu, W.; Zhou, Y.; Sun, D.; Li, Z. An uPA Cleavable Conjugate of a Recombinant $\alpha v\beta 3$ Targeting Toxin and Its Bioactivity. *World J. Microbiol. Biotechnol.* **2011**, *27*, 563–569.
11. Pan, H.; Myerson, J. W.; Ivashyna, O.; Soman, N. R.; Marsh, J. N.; Hood, J. L.; Lanza, G. M.; Schlesinger, P. H.; Wickline, S. A. Lipid Membrane Editing with Peptide Cargo Linkers in Cells and Synthetic Nanostructures. *FASEB J.* **2010**, *24*, 2928–2937.
12. Russell, P.; Hewish, D.; Carter, T.; Sterling-Levis, K.; Ow, K.; Hattarki, M.; Doughty, L.; Guthrie, R.; Shapira, D.; Molloy, P.; *et al*. Cytotoxic Properties of Immunoconjugates Containing Melittin-Like Peptide 101 against Prostate Cancer: *In Vitro* and *in Vivo* Studies. *Cancer Immunol. Immunother.* **2004**, *53*, 411–421.
13. Werkmeister, J. A.; Kirkpatrick, A.; McKenzie, J. A.; Rivett, D. E. The Effect of Sequence Variations and Structure on the Cytolytic Activity of Melittin Peptides. *Biochim. Biophys. Acta, Gen. Subj.* **1993**, *1157*, 50–54.
14. Zhao, X.; Yu, Z.; Dai, W.; Yao, Z.; Zhou, W.; Zhou, W.; Zhou, J.; Yang, Y.; Zhu, Y.; Chen, S.; *et al*. Construction and Characterization of an Anti-Asialoglycoprotein Receptor Single-Chain Variable-Fragment-Targeted Melittin. *Biotechnol. Appl. Biochem.* **2011**, *58*, 405–411.
15. Dunn, R. D.; Weston, K. M.; Longhurst, T. J.; Lilley, G. G.; Rivett, D. E.; Hudson, P. J.; Raison, R. L. Antigen Binding and Cytotoxic Properties of a Recombinant Immunotoxin Incorporating the Lytic Peptide, Melittin. *Immunotechnology* **1996**, *2*, 229–240.
16. Zetterberg, M. M.; Reijmar, K.; Pränting, M.; Engström, Å.; Andersson, D. I.; Edwards, K. PEG-Stabilized Lipid Disks as Carriers for Amphiphilic Antimicrobial Peptides. *J. Controlled Release* **2011**, *156*, 323–328.
17. Yang, L.; Cui, F.; Shi, K.; Cun, D.; Wang, R. Design of High Payload PLGA Nanoparticles Containing Melittin/Sodium Dodecyl Sulfate Complex by the Hydrophobic Ion-Pairing Technique. *Drug Dev. Ind. Pharm.* **2009**, *35*, 959–968.
18. Dang, Y.-Q.; Li, H.-W.; Wu, Y. Construction of a Supramolecular Förster Resonance Energy Transfer System and Its Application Based on the Interaction between Cy3-Labeled Melittin and Phosphocholine Encapsulated Quantum Dots. *ACS Appl. Mater. Interfaces* **2012**, *4*, 1267–1272.
19. Torchilin, V. P. Recent Advances with Liposomes as Pharmaceutical Carriers. *Nat. Rev. Drug Discovery* **2005**, *4*, 145–160.
20. Popplewell, J. F.; Swann, M. J.; Freeman, N. J.; McDonnell, C.; Ford, R. C. Quantifying the Effects of Melittin on Liposomes. *Biochim. Biophys. Acta, Biomembr.* **2007**, *1768*, 13–20.
21. Soman, N. R.; Lanza, G. M.; Heuser, J. M.; Schlesinger, P. H.; Wickline, S. A. Synthesis and Characterization of Stable Fluorocarbon Nanostructures as Drug Delivery Vehicles for Cytolytic Peptides. *Nano Lett.* **2008**, *8*, 1131–1136.
22. Soman, N. R.; Baldwin, S. L.; Hu, G.; Marsh, J. N.; Lanza, G. M.; Heuser, J. E.; Arbeit, J. M.; Wickline, S. A.; Schlesinger, P. H. Molecularly Targeted Nanocarriers Deliver the Cytolytic Peptide Melittin Specifically to Tumor Cells in Mice, Reducing Tumor Growth. *J. Clin. Invest.* **2009**, *119*, 2830–2842.
23. Cabral, H.; Matsumoto, Y.; Mizuno, K.; Chen, Q.; Murakami, M.; Kimura, M.; Terada, Y.; Kano, M. R.; Miyazono, K.; Uesaka, M.; *et al*. Accumulation of Sub-100 nm Polymeric Micelles in Poorly Permeable Tumours Depends on Size. *Nat. Nanotechnol.* **2011**, *6*, 815–823.
24. Minchinton, A. I.; Tannock, I. F. Drug Penetration in Solid Tumours. *Nat. Rev. Cancer* **2006**, *6*, 583–592.
25. Pluen, A.; Boucher, Y.; Ramanujan, S.; McKee, T. D.; Gohongi, T.; di Tomaso, E.; Brown, E. B.; Izumi, Y.; Campbell, R. B.; Berk, D. A.; *et al*. Role of Tumor-Host Interactions in Interstitial Diffusion of Macromolecules: Cranial *vs.* Subcutaneous Tumors. *Proc. Natl. Acad. Sci. U.S.A.* **2001**, *98*, 4628–4633.
26. Zhang, Z.; Cao, W.; Jin, H.; Lovell, J. F.; Yang, M.; Ding, L.; Chen, J.; Corbin, I.; Luo, Q.; Zheng, G. Biomimetic Nanocarrier for Direct Cytosolic Drug Delivery. *Angew. Chem., Int. Ed.* **2009**, *48*, 9171–9175.
27. Navab, M.; Anantharamaiah, G.; Reddy, S. T.; Hama, S.; Hough, G.; Grijalva, V. R.; Yu, N.; Ansell, B. J.; Datta, G.; Garber, D. W. Apolipoprotein A-I Mimetic Peptides. *Arterioscler., Thromb., Vasc. Biol.* **2005**, *25*, 1325–1331.
28. Zheng, Y.; Huang, C.; Cheng, Z.; Chen, M. Establishment of Visible Animal Metastasis Models for Human Nasopharyngeal Carcinoma Based on a Far-Red Fluorescent Protein. *J. Innov. Opt. Health Sci.* **2012**, *05*, 1250019.
29. Habermann, E.; Zeuner, G. Comparative Studies of Native and Synthetic Melittins. *Naunyn-Schmiedebergs Arch. Pharmak.* **1971**, *270*, 1–9.
30. Zheng, Y.; Liu, Y.; Jin, H.; Pan S.; Qian Y.; Huang, C.; Zeng, Y.; Luo, Q.; Zeng, M.; Zhang, Z. Scavenger Receptor B1 Is a Potential Biomarker of Human Nasopharyngeal Carcinoma and Its Growth Is Inhibited by HDL-Mimetic Nanoparticles. *Theranostics*, **2013**, *3*, 477−486.
31. Giraud, F.; Claret, M.; Garay, R. Interactions of Cholesterol with the Na Pump in Red Blood Cells. *Nature* **1976**, *264*, 646–648.
32. Zhang, Z.; Chen, J.; Ding, L.; Jin, H.; Lovell, J. F.; Corbin, I. R.; Cao, W.; Lo, P.-C.; Yang, M.; Tsao, M.-S.; *et al*. HDL-Mimicking Peptide−Lipid Nanoparticles with Improved Tumor Targeting. *Small* **2010**, *6*, 430–437.
33. Cormode, D. P.; Frias, J. C.; Ma, Y.; Chen, W.; Skajaa, T.; Briley-Saebo, K.; Barazza, A.; Williams, K. J.; Mulder, W. J. M.; Fayad, Z. A.; *et al*. HDL as a Contrast Agent for Medical Imaging. *Clin. Lipidol.* **2009**, *4*, 493–500.
34. Yang, M.; Chen, J.; Cao, W.; Ding, L.; Ng, K. K.; Jin, H.; Zhang, Z.; Zheng, G. Attenuation of Nontargeted Cell-Kill Using a High-Density Lipoprotein-Mimicking Peptide−Phospholipid Nanoscaffold. *Nanomedicine* **2011**, *6*, 631–641.
35. Pelaz, B.; Jaber, S.; de Aberasturi, D. J.; Wulf, V.; Aida, T.; de la Fuente, J. M.; Feldmann, J.; Gaub, H. E.; Josephson, L.; Kagan, C. R.; *et al*. The State of Nanoparticle-Based Nanoscience and Biotechnology: Progress, Promises, and Challenges. *ACS Nano* **2012**, *6*, 8468–8483.
36. Krieger, M.; Anderson, R. G. W.; Goldstein, J. L.; Brown, M. S.; Smith, L. C.; Kao, Y. J.; Pownall, H. J.; Gotto Jr., A. M. Reconstituted Low Density Lipoprotein: A Vehicle for the Delivery of Hydrophobic Fluorescent Probes to Cells. *J. Supramol. Struct.* **1979**, *10*, 467–478.
37. Yang, X.; Gong, H.; Fu, J.; Quan, G.; Huang, C.; Luo, Q. Molecular Imaging of Small Animals with Fluorescent Proteins: From Projection to Multimodality. *Comput. Med. Imaging Graphics* **2012**, *36*, 259–263.
38. Luo, H.; Yang, J.; Jin, H.; Huang, C.; Fu, J.; Yang, F.; Gong, H.; Zeng, S.; Luo, Q.; Zhang, Z. Tetrameric Far-Red Fluorescent Protein as a Scaffold to Assemble an Octavalent Peptide Nanoprobe for Enhanced Tumor Targeting and Intracellular Uptake *in Vivo*. *FASEB J.* **2011**, *25*, 1865–1873.